Current Biology, Volume *22*

Supplemental Information

Shaping of Object Representations in the Human Medial Temporal Lobe Based on Temporal Regularities

Anna C. Schapiro, Lauren V. Kustner, and Nicholas B. Turk-Browne

Supplemental Inventory

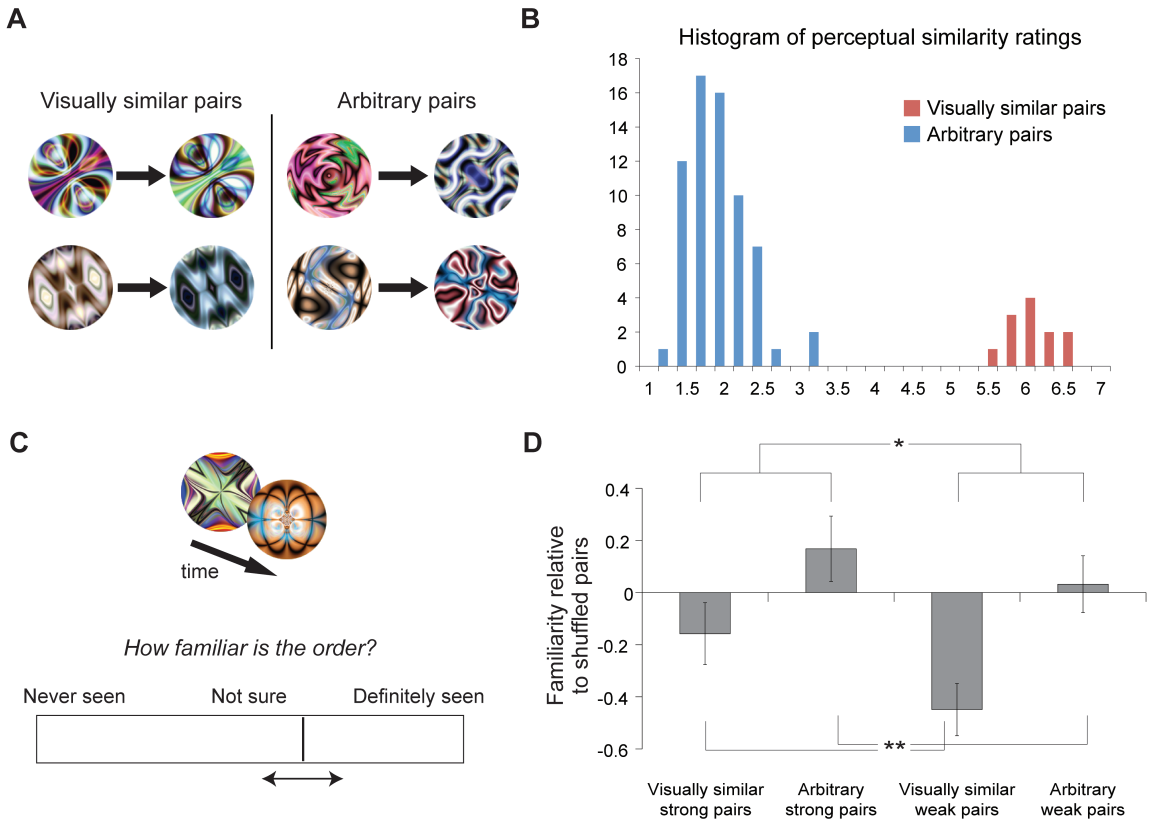

Figure S1. Full Procedure, Related to Figure 1

(A) Our study focused on pairs of fractals with arbitrary visual similarity since, relative to a baseline of also arbitrary shuffled pairs, their representations should not be more similar for any reason other than their temporal co-occurrence. However, we also included some pairs whose members were chosen to be highly visually similar as an initial exploration of how the pre-existing similarity of representations might influence learning about regularities. For each subject, four fractals were used as the base member of visually similar pairs, where the other member was simply a color inverse. Thus, the two fractals in a pair had identical textures and shape contours. These pairs were divided into strong and weak transition probabilities, as for arbitrary pairs.

(B) To confirm that our manipulation of visual similarity was effective, we ran a Mechanical Turk study in which 24 subjects rated arbitrary and visually similar pairs on the perceived similarity of their members (each subject rated all 78 possible pairs, the majority of which were arbitrary). The scale ranged from 1 ("completely different") to 7 ("nearly identical"). Comparing the distributions of responses, the visually similar pairs were perceived as much more similar than the arbitrary pairs ($t[76]=39.04$, $p<.001$).

(C) To assess behavioral learning in this paradigm, we conducted a pilot study outside of the scanner. Twelve subjects were exposed to the same stimulus parameters as in the fMRI experiment, except without a randomly ordered run at the end. We included the randomly ordered run at the beginning as practice for the task of detecting grayscale patches. After sequence exposure, subjects completed a familiarity test in which two fractals were presented sequentially. These two fractals could belong to a strong pair, weak pair, or shuffled pair. Subjects rated how familiar the order of the fractals seemed using a sliding bar.

(D) There was a main effect of transition probability strength, with strong pairs rated as more familiar than weak pairs ($F[1,11]=5.78$, $p=.035$). There was also a main effect of similarity, with visually similar pairs rated as less familiar than arbitrary pairs ($F[1,11]=11.45$, $p=.006$; see Fig. S2 for a potential explanation). There was no interaction between probability strength and similarity ($F[1,11]=1.66$, $p=.225$). *$p<.05$; **$p<.01$. Error bars denote ± 1 SEM.

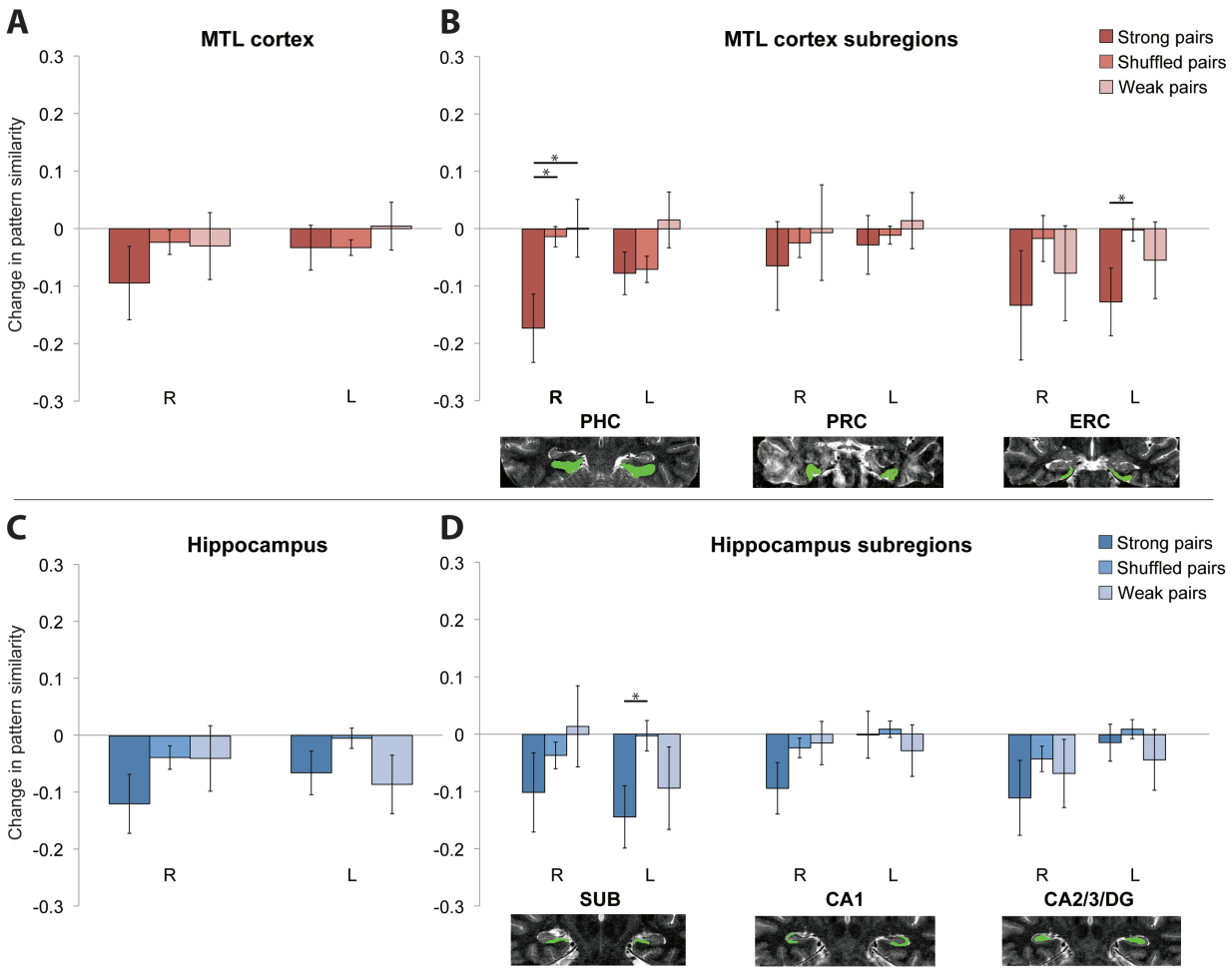

Figure S2. ROI Results for Visually Similar Pairs, Related to Figure 2

(A) In bilateral MTL cortex, the visually similar pairs did not show any reliable changes in pattern similarity from before to after learning for strong vs. shuffled pairs, weak vs. shuffled pairs, or strong vs. weak pairs (*t*s<1).

(B) In bilateral MTL subregions, the pattern correlation for strong pairs *decreased* from before to after learning relative to shuffled pairs in PHC (*t*[16]=-2.27, *p*=.038) and marginally in ERC (*t*[16]=-1.87, *p*=.080), but did not change in PRC (*t*<1). This decrease was greater for strong vs. weak pairs in PHC (*t*<[16]=-2.67, *p*=.017), but not in PRC or ERC (*t*s<1). The weak pairs did not differ from shuffled pairs in PHC (*t*[16]=1.33, *p*=.203), PRC (*t*<1), or ERC (*t*[16]=-1.07, *p*=.299).

(C) In bilateral hippocampus, the visually similar pairs showed a marginal decrease in pattern similarity from before to after learning for strong vs. shuffled pairs (*t*[16]=-1.95, *p*=.069), but no change for strong vs. weak pairs or weak vs. shuffled pairs (*t*s<1).

(D) In bilateral hippocampal subfields, the pattern correlation for strong pairs decreased from before to after learning relative to shuffled pairs in subiculum (SUB; *t*[16]=-2.31, *p*=.034), but did not change in CA1 (*t*[16]=-1.28, *p*=.220) or CA2/3/DG (*t*[16]=-1.09, *p*=.294). There was no difference between strong and weak visually similar pairs in any subfield (*t*s<1), nor were weak pairs different from shuffled pairs (*t*s<1).

Within each hemisphere, strong pairs decreased from before to after learning in right PHC, left ERC, and left SUB (stars indicate significant effects). This decrease was greater for the strong vs. weak pairs in right PHC. One potential explanation for the *differentiation* of representations from visually similar

strong pairs is that these items were so similar that they were not perceived as distinct objects at the beginning of the experiment. With greater exposure to these fractals, especially when appearing consecutively in strong pairs, subjects may have been better able to discriminate the subtle color differences. Indeed, seven subjects did not report noticing any similar-looking fractals during sequence exposure, despite seeing visually similar strong pairs about 40 times each. We tested two further predictions that arise from these differentiation findings: First, insofar as perceptual similarity leads to decreased pattern similarity with statistical learning, we might expect that *arbitrary* pairs with relatively high similarity would show attenuated increases compared to arbitrary pairs with relatively low similarity. To test this hypothesis, we ran another Mechanical Turk study with 65 subjects to assess the perceived similarity of just the arbitrary pairs (the visually similar pairs in the previous survey may have compressed the range of responses; we also changed response 7 to "very similar" since all pairs were fairly dissimilar now). Using these aggregate survey responses, we computed the average perceptual similarity of the members of each arbitrary pair that fMRI subjects were exposed to (resulting in a perceptual similarity score for each subject). If perceptual similarity drives differentiation, then there should be a negative correlation across subjects between this score and the increase in pattern correlation from before to after learning for the strong arbitrary pairs. This exact pattern was found in CA1 (r[15]=-.511, p=.036) and CA2/3/DG (r[15]=-.639, p=.006), and marginally in ERC (r[15]=-.441, p=.076); but not in the remaining subregions (ps>.13). The second prediction arising from differentiation is that members of visually similar pairs should be less confusable behaviorally after learning. To test this prediction, 42 subjects were exposed to the same temporal regularities as in the fMRI study but again without a final random run. They then completed 80 trials of a numerosity discrimination task over rapid serial visual presentation streams of 20 fractals (100 ms duration each, no ISI). Every stream contained four different fractals, two from one strong or weak pair and two from one shuffled pair, each repeated a varying number of times in a randomized order. If the pair used in a stream was visually similar, the shuffled pair consisted of a fractal from an arbitrary pair and its (new) color inverse (to equate the similarity within pairs and shuffled pairs). After each stream, two fractals from the stream were presented as a test probe (one each from the pair and shuffled pair). Subjects were asked to decide which of these two images they had seen more often in the stream. We hypothesized that if the representations of visually similar pairs had differentiated, the members of these pairs should be less confusable than the (visually similar) fractals in the shuffled pair. This might lead to *underestimation* of the frequency of pair vs. shuffled pair members, since the shuffled pair test probe's mate should be relatively more likely to be counted as the test probe. We quantified a bias index as the proportion of trials in which the pair member was chosen (chance=.5). As expected, we found a reliable underestimation bias for visually similar strong (M=.454, SD=.111; t[41]=-2.72, p=.010) and weak pairs (M = .445, SD = .120; t[41]=-2.96, p=.005). *p<.05;. Error bars denote ± 1 SEM.

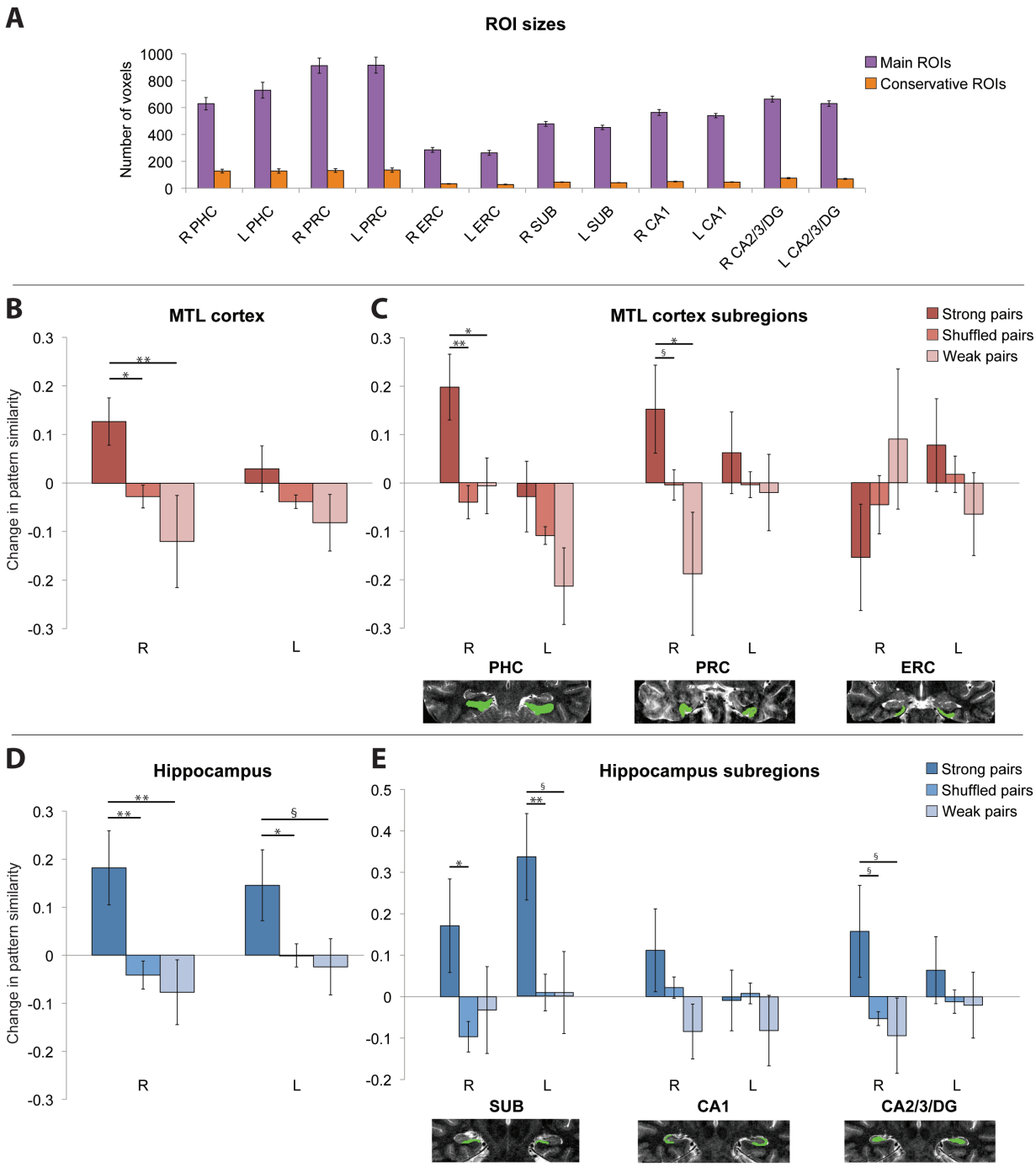
A
ROI sizes
Number of voxels
1000
800
600
400
200
0
Main ROIs
Conservative ROIs
R PHC
L PHC
R PRC
L PRC
R ERC
L ERC
R SUB
L SUB
R CA1
L CA1
R CA2/3/DG
L CA2/3/DG
B
MTL cortex
Change in pattern similarity
0.3
0.2
0.1
0
-0.1
-0.2
-0.3
R
L
C
MTL cortex subregions
Strong pairs
Shuffled pairs
Weak pairs
PHC
PRC
ERC
D
Hippocampus
E
Hippocampus subregions
0.5
0.4
SUB
CA1
CA2/3/DG

Figure S3. Conservative ROI Results, Related to Figure 3

There is a trade-off between confidence that functional voxels come from a particular ROI and the number of voxels available for analysis in that ROI. The results presented in the main text reflect our *a priori* decision about the level of confidence to use. We re-analyzed our data using a very stringent definition of when a functional voxel should be considered as belonging to an ROI. After registering the binary mask for each MTL ROI (and the functional data) into standard 2 mm space, we obtained a graded map in which each voxel contained a value in [0,1], roughly reflecting the degree to which it belonged to the ROI. This image was then thresholded using an adaptive procedure in which the 90th percentile of the robust range of non-zero values was estimated and everything below that value was zeroed-out. This highly conservative threshold shrunk the size of the ROIs considerably, limiting ROIs to only the most central voxels (i.e., voxels that neighbored many other voxels with the same label). Overall, the pattern of results from these conservative ROIs was very similar to those from the main ROIs, lending support to our attribution of the main results to specific ROIs.

(A) Number of voxels (in 2 x 2 x 2 mm standard space) in the main (Fig. 2) and conservative ROIs. Across subregions, increases in pattern similarity for strong vs. shuffled pairs were uncorrelated with the sizes of both the main (r=.151, p=.64) and conservative (r=.154, p=.63) ROIs. Within subregions, pattern similarity was generally robust to the reduced number of voxels in the conservative ROIs.

(B) In bilateral MTL cortex, the pattern correlation for fractals from strong pairs increased from before to after learning relative to shuffled pairs (t[16]=2.74, p=.014). This increase was greater than for weak pairs (t[16]=2.79, p=.013), which in turn did not differ from shuffled pairs (t[16]=-1.38, p=.185).

(C) In bilateral MTL subregions, the pattern correlation for strong pairs increased from before to after learning in PHC (t[16]=3.13, p=.007) and PRC (t[16]=2.29, p=.036), but not ERC (t<1). This increase was greater for strong vs. weak pairs in PHC (t[16]=2.69, p=.016) and PRC (t[16]=2.49, p=.024), but not ERC (t<1). The weak pairs did not differ from shuffled pairs in PHC (t<1), PRC (t[16]=-1.40, p=.180), or ERC (t<1).

(D) In bilateral hippocampus, the pattern correlation for fractals from strong pairs increased from before to after learning relative to shuffled pairs (t[16]=3.54, p=.003). This increase was greater than for weak pairs (t[16]=2.85, p=.012), which in turn did not differ from shuffled pairs (t<1).

(E) In bilateral hippocampal subfields, the pattern correlation for strong pairs increased from before to after learning in SUB (t[16]=3.78, p=.002) and CA2/3/DG (t[16]=2.61, p=.019), but not CA1 (t<1). This increase was greater for strong vs. weak pairs in CA2/3/DG (t[16]=2.60, p=.019), and marginally greater in SUB (t[16]=2.03, p=.059) and CA1 (t[16]=1.90, p=.076). The weak pairs did not differ from shuffled pairs in SUB or CA2/3/DG (ts<1), but there was a marginal decrease in CA1 (t[16]=-2.04, p=.058).

The lack of an increase for strong vs. shuffled pairs in CA1 is the only discrepancy between this analysis and the main analysis. Note that this was probably not a result of CA1 being a small ROI per se, since some of the strongest effects occurred in SUB, which had a smaller number of voxels on average. Nevertheless, the increase for strong vs. weak pairs in CA1 persisted as a marginal effect. Thus, despite a large reduction in the size of the ROIs, we replicated the increased pattern similarity for strong vs. shuffled pairs in four of the five regions that showed this effect in the main analysis, as well as the increased pattern similarity for strong vs. weak pairs in all five regions that showed this effect in the main analysis with at least marginal significance. §p<.1; *p<.05; **p<.01. Error bars denote ± 1 SEM.

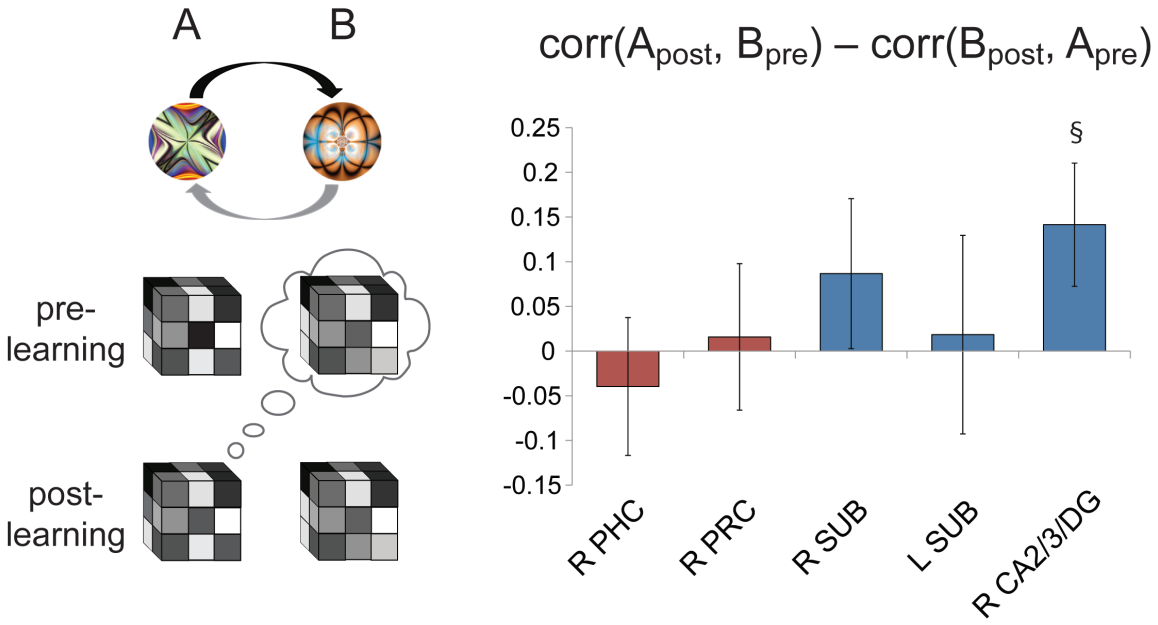

Figure S4. Asymmetry Results for Conservative ROIs, Related to Figure 4

We re-ran the prediction vs. association analysis for the conservative ROIs that showed at least marginal increases for strong vs. shuffled pairs (Fig. S3). Right CA2/3/DG showed the only reliable (marginal) effect, consistent with predictive bias of this ROI in the main analysis. §$p<.1$. Error bars denote ± 1 SEM.

Table S1. Exploratory Searchlight Results outside of the MTL, Related to Figure 3

Region	Corrected *p* value	Center-of-gravity MNI			Extent (voxels)
		x	*y*	*z*	
Anterior temporal lobe	.014	43	11	-21	86
Thalamus	.002	-3	-7	14	187
Cerebellum	.018	-4	-40	-2	81
Anterior cingulate cortex/Caudate	.002	-2	18	-4	191

Our acquisition parameters did not provide adequate coverage of the whole brain. Nevertheless, as an exploratory analysis we examined pattern similarity outside of the MTL using searchlights. The searchlight analysis was nearly identical to the one performed within MTL, except that subjects' brains were aligned using standard registration techniques. Voxelwise reliability was again assessed with *randomise*, but the resulting statistical maps were additionally corrected for multiple comparisons. Specifically, a corrected p-value was assigned to each cluster by assessing its size with respect to the null distribution of the maximum cluster mass during the permutation simulations (cluster-forming threshold $p<.001$). Four voxel clusters showed a greater increase in pattern correlation from before to after learning for strong vs. weak pairs ($p<.05$, corrected): right anterior temporal lobe (ATL), bilateral thalamus, left cerebellum, and a midline cluster including anterior cingulate cortex and caudate. In non-human primates, more ventral aspects of ATL are interconnected with PRC and have been linked to visual associative learning [1]. The caudate has also been implicated in related forms of learning [2], including artificial grammar learning [3], classification learning [4], and statistical learning [5]. How MTL, lateral ATL, and striatum interact to represent regularities is an important question for future work.

Supplemental Experimental Procedures

Subjects

Twenty participants (14 females, mean age 20.5 years, range 18-30 years) from the Princeton University community were recruited in exchange for monetary compensation or course credit. Data from three subjects were unusable due to technical issues. Informed consent was obtained from all subjects, and the study protocol was approved by the Institutional Review Board for Human Subjects at Princeton University.

Stimuli and Design

Fractal-like images were created in ArtMatic Pro (www.artmatic.com). For each subject, the 16 fractals were randomly assigned to be the first or second member of pairs. There were two pairs in each of the strong and weak conditions (Fig. 1), and two additional pairs in each of two visual manipulation conditions that are not relevant for present purposes (Figs. S1, S2). Each of ten five-minute runs contained a continuous sequence of 80 fractals. The order of fractals in the first and last runs was pseudo-randomized: individual fractals were drawn without replacement to generate the first 16 trials, again to create the next 16 trials, and so on. The same pseudo-random order was used in the first and last run for each subject to equate any spurious order effects or biases in modeling the fMRI response for trials before and after learning. In the eight intervening runs, the order of fractals was generated by choosing pairs pseudo-randomly, such that each fractal appeared with equal frequency on average and no pair appeared twice in a row. For strong pairs, the first member of the pair was always followed by the second member of the pair. For weak pairs, the first member of the pair was followed by the second member of the pair only one-third of the time. To equate the frequency of members from weak pairs, the second member was inserted into the trial sequence on its own for the remaining two-thirds of the time.

Fractal images subtended 4.5 degrees of visual angle in diameter, and were presented for 1s each, with an ISI of 1, 3, or 5s (40%, 40%, and 20% of trials, respectively). This jitter served two purposes: First, it obscured the pair structure, since a pair member often occurred closer in time to a member of a different pair than to its own mate. Second, when modeling the BOLD response in the first and last (random) runs, it allowed us to better statistically separate the responses to individual trials. Because the trial sequence was continuous, there were no grouping or segmentation cues to the pair structure other than the temporal regularities.

Procedure

During all functional runs, subjects used a button box to make a judgment about whether each fractal contained a grayscale patch. Specifically, the fractal images were fully colored, but on a random 10% of trials, the images were distorted by rendering about 1/6 of the area grayscale. Subjects responded on every trial, indicating whether they saw a grayscale patch or not. If they responded correctly, a white fixation dot in the middle of the fractal would turn green. If they responded incorrectly, it would turn red. Response mappings were randomized across subjects.

Data Acquisition

Data were acquired using a 3T Siemens Allegra scanner with a volume head coil. We collected 10 functional runs with a T2*-weighted gradient-echo EPI sequence (TE=28 ms; TR=2000 ms; FA=71°; matrix=64×64). Thirty-five oblique coronal slices were aligned perpendicular to the

anterior-posterior axis of the hippocampus (2×2 mm inplane, 3 mm thickness), optimizing coverage for MTL. Each run contained 158 volumes. We collected two anatomical runs for registration across subjects to standard space: a coplanar T1-weighted FLASH sequence and a high-resolution 3D T1-weighted MPRAGE sequence. For manual segmentation of MTL ROIs, we collected an additional high-resolution coplanar T2-weighted TSE sequence (35 slices; 0.5×0.5 mm inplane, 3mm thickness). Similar imaging parameters have been used in other studies of the MTL [6-12].

MTL Segmentation

For each subject, PHC, PRC, ERC, subiculum, CA1, and CA2/3/DG were hand-segmented in each hemisphere on the T2-weighted TSE images based on anatomical landmarks [13-17]. Considering our voxel size and slice angle, the anterior border of PRC begins at the anterior-most slice where the collateral sulcus (CoS) is visible. The posterior border of PRC (the boundary between PRC and PHC) is the most posterior slice that includes the hippocampal head. The lateral border of PRC is at the base of the lateral bank of CoS. The medial border of PRC (and the lateral border of ERC) starts at the base of the medial bank of CoS at the anterior border, and moves laterally halfway up the medial bank before receding back in the medial direction at the posterior border. The anterior border of ERC begins the slice posterior to the first appearance of the frontotemporal junction. The posterior border of ERC is the slice anterior to the posterior border of PRC. The medial border of ERC is the projected continuation of the inferior boundary of the hippocampus, perpendicular to the gray matter ribbon. The anterior border of PHC is one slice posterior to the posterior-most slice of the hippocampal head, and the posterior border is the last slice where the hippocampal formation is identifiable. The lateral border of PHC is the same as the lateral border of PRC and the medial border is halfway up and perpendicular to the gray matter bend. Subiculum, CA1, and CA2/3/DG run anterior to posterior in all slices that the hippocampal formation is visible. CA2/3/DG fills the majority of the coronal slice of the hippocampus and contains CA2, CA3, and DG subfields (not separable with current MRI resolution and contrast). CA1 wraps around the lateral edge from dorsal to ventrolateral aspects of CA2/3/DG. The subiculum fills a ventral sliver of the hippocampus. Moving anterior to posterior, the medial boundary of the subiculum borders ERC, PRC and PHC, respectively, and the ventrolateral boundary with CA1 becomes increasingly medial.

fMRI Preprocessing

Functional runs were preprocessed with FEAT 5.98 in FSL (www.fmrib.ox.ac.uk/fsl), including: motion correction using MCFLIRT; slice-timing correction using Fourier-space timeseries phase-shifting; non-brain removal using BET; highpass temporal filtering using a 64s-sigma Gaussian kernel; and spatial smoothing using a 5mm FWHM Gaussian kernel. This smoothing kernel roughly matches the point-spread function of 3T gradient-echo EPI data [18], and thus reduces noise under the matched filter theorem. Moreover, moderate spatial smoothing does not seem to negatively affect correlation-based MVPA, even for signals at a small spatial scale [19]. Regardless, we replicated our pattern of results using no spatial smoothing during preprocessing. Functional runs were registered with FLIRT to the FLASH image, the MPRAGE image, and an MNI standard brain with interpolation to 2mm isotropic voxels. Because MTL ROIs were segmented at a higher anatomical resolution, the ROI labels for functional voxels were inherently ambiguous. To be more confident that our results reflect specific subregions, we repeated all

analyses using only functional voxels that were in the 90th percentile in terms of likelihood of belonging to the segmented ROI (Figs. S3, S4).

fMRI Analyses

General Linear Modeling

Before conducting pattern analyses, we modeled the evoked response to individual fractals in the first and last runs of the experiment. The GLM was fit using FILM and local autocorrelation correction in FSL. The regressor for each of 16 fractals contained a delta function at every repetition convolved with a double-gamma hemodynamic response function. The fractals from the visual manipulation pairs were included so that their evoked responses did not influence the parameter estimates of the arbitrarily paired fractals of interest. The resulting parameter estimates reflected the response of all voxels to each fractal before and after learning.

ROI Analyses

The parameter estimates for all voxels in each ROI were extracted and arranged into a vector. Pattern similarity was assessed by computing the Pearson correlation of vectors corresponding to different fractals. The resulting coefficients were Fisher transformed for statistical analysis. Three different correlations were calculated for each subject: (1) the mean correlation of the two members from each of the two strong pairs, (2) the mean correlation of the two members from each of the two weak pairs, and (3) the mean correlation of all combinations of two fractals that were neither strong nor weak pairs. The latter shuffled pairs were used as a resampled baseline to assess how pattern similarity changed as a result of our procedure in the absence of the possibility for statistical learning. The visual manipulation fractals were included in this baseline to increase statistical power, although the pattern of results was identical when they were excluded.

For the primary analysis of how pattern similarity changed as a result of learning, we subtracted the shuffled pair baseline correlation from the strong or weak pair correlation both before and after sequence exposure, and then in turn subtracted the before-learning difference from the after-learning difference. That is, we calculated how much the pattern similarity for strong and weak pairs increased from before to after learning relative to shuffled pairs. We also compared the magnitude of changes for strong and weak pairs with paired t-tests.

In the main analyses, members of a pair were correlated at a single stage of the experiment (i.e., either both after or both before learning). To examine whether increases in pattern similarity reflected associative changes (whereby both members became more similar to each other) vs. predictive changes (whereby the first member became more similar to the second, but not vice versa), we correlated the vector for one member of a pair after learning (post) with the vector for the other member of the pair before learning (pre), and then repeated the procedure switching the after/before labels. Insofar as one member of the pair changed more than the other, then the difference between these correlations should be reliable. For example, if A and B were members of a strong pair in which A always preceded B, asymmetric changes in the forwards direction would be supported by a higher correlation for A_{post}/B_{pre} than for B_{post}/A_{pre}.

Searchlight Analyses

The analyses above used patterns defined over all voxels in an ROI, and may thus be most sensitive to representations that are distributed across the extent of the ROI. However, smaller subregions of an ROI may have exhibited robust changes, indicative of more localized representations. Examining subregions presents an additional difficulty in terms of how to assess statistical reliability across subjects. Specifically, when looking over entire ROIs, subjects' brains did not need to be in the same space. For each analysis, we simply had one correlation coefficient or difference per subject and ROI. In contrast, the searchlight analyses of ROI subregions described below produce voxelwise maps of correlation coefficients for each subject and ROI. These maps must be aligned into the same space so that reliability can be assessed on a voxel-by-voxel basis and attributed to particular subregions.

Because MTL subregions are very small and variable in size and location across subjects, we used a non-linear deformation routine from the Advanced Normalization Techniques toolbox (http://picsl.upenn.edu/ANTS) to generate a group template MTL. In the template, voxels were assigned to the label that matched the highest proportion of subjects, considering only labels found in at least 1/3 of subjects for a given voxel. We applied the transformation obtained by aligning each subject's ROIs into template space to the pattern of GLM parameter estimates for each fractal. For every subject, we then swept a 27-voxel cubic searchlight throughout each template ROI [20], performing the same pattern analyses as in the entire ROIs. For searchlights at the edge of ROIs that had fewer than 27 voxels, correlations were calculated with fewer voxels. Because identical searchlights were used before and after learning, searchlight size and other analysis choices cannot explain changes in pattern correlation and/or differences between conditions. We assigned the final statistic value (the increase in pattern similarity for strong vs. weak pairs) to the center voxel of each searchlight. To test the reliability of these statistics across subjects, we used the *randomise* function in FSL to perform permutation tests.

Supplemental References

1. Yoshida, M., Naya, Y., and Miyashita, Y. (2003). Anatomical organization of forward fiber projections from area TE to perirhinal neurons representing visual long-term memory in monkeys. Proc Natl Acad Sci U S A *100*, 4257-4262.
2. Shohamy, D. (2011). Learning and motivation in the human striatum. Curr Opin Neurobiol *21*, 408-414.
3. Lieberman, M.D., Chang, G.Y., Chiao, J., Bookheimer, S.Y., and Knowlton, B.J. (2004). An event-related fMRI study of artificial grammar learning in a balanced chunk strength design. J Cogn Neurosci *16*, 427-438.
4. Seger, C.A., and Cincotta, C.M. (2005). The roles of the caudate nucleus in human classification learning. J Neurosci *25*, 2941-2951.
5. Turk-Browne, N.B., Scholl, B.J., Chun, M.M., and Johnson, M.K. (2009). Neural evidence of statistical learning: efficient detection of visual regularities without awareness. J Cogn Neurosci *21*, 1934-1945.
6. Zeineh, M.M., Engel, S.A., Thompson, P.M., and Bookheimer, S.Y. (2003). Dynamics of the hippocampus during encoding and retrieval of face-name pairs. Science *299*, 577-580.

7. Chen, J., Olsen, R.K., Preston, A.R., Glover, G.H., and Wagner, A.D. (2011). Associative retrieval processes in the human medial temporal lobe: hippocampal retrieval success and CA1 mismatch detection. Learn Mem *18*, 523-528.
8. Dudukovic, N.M., Preston, A.R., Archie, J.J., Glover, G.H., and Wagner, A.D. (2011). High-resolution fMRI reveals match enhancement and attentional modulation in the human medial temporal lobe. J Cogn Neurosci *23*, 670-682.
9. Eldridge, L.L., Engel, S.A., Zeineh, M.M., Bookheimer, S.Y., and Knowlton, B.J. (2005). A dissociation of encoding and retrieval processes in the human hippocampus. J Neurosci *25*, 3280-3286.
10. Suthana, N., Ekstrom, A., Moshirvaziri, S., Knowlton, B., and Bookheimer, S. (2011). Dissociations within human hippocampal subregions during encoding and retrieval of spatial information. Hippocampus *21*, 694-701.
11. Olsen, R.K., Nichols, E.A., Chen, J., Hunt, J.F., Glover, G.H., Gabrieli, J.D., and Wagner, A.D. (2009). Performance-related sustained and anticipatory activity in human medial temporal lobe during delayed match-to-sample. J Neurosci *29*, 11880-11890.
12. Preston, A.R., Bornstein, A.M., Hutchinson, J.B., Gaare, M.E., Glover, G.H., and Wagner, A.D. (2010). High-resolution fMRI of content-sensitive subsequent memory responses in human medial temporal lobe. J Cogn Neurosci *22*, 156-173.
13. Pruessner, J.C., Kohler, S., Crane, J., Pruessner, M., Lord, C., Byrne, A., Kabani, N., Collins, D.L., and Evans, A.C. (2002). Volumetry of temporopolar, perirhinal, entorhinal and parahippocampal cortex from high-resolution MR images: considering the variability of the collateral sulcus. Cereb Cortex *12*, 1342-1353.
14. Duvernoy, H. (1998). The Human Hippocampus, (New York: Springer-Verlag).
15. Carr, V.A., Rissman, J., and Wagner, A.D. (2010). Imaging the human medial temporal lobe with high-resolution fMRI. Neuron *65*, 298-308.
16. Insausti, R., Juottonen, K., Soininen, H., Insausti, A.M., Partanen, K., Vainio, P., Laakso, M.P., and Pitkanen, A. (1998). MR volumetric analysis of the human entorhinal, perirhinal, and temporopolar cortices. Am J Neuroradiol *19*, 659-671.
17. Ding, S.L., Van Hoesen, G.W., Cassell, M.D., and Poremba, A. (2009). Parcellation of human temporal polar cortex: a combined analysis of multiple cytoarchitectonic, chemoarchitectonic, and pathological markers. J Comp Neurol *514*, 595-623.
18. Parkes, L.M., Schwarzbach, J.V., Bouts, A.A., Deckers, R.H., Pullens, P., Kerskens, C.M., and Norris, D.G. (2005). Quantifying the spatial resolution of the gradient echo and spin echo BOLD response at 3 Tesla. Magn Reson Med *54*, 1465-1472.
19. Op de Beeck, H.P. (2010). Against hyperacuity in brain reading: spatial smoothing does not hurt multivariate fMRI analyses? NeuroImage *49*, 1943-1948.
20. Pereira, F., and Botvinick, M. (2011). Information mapping with pattern classifiers: a comparative study. NeuroImage *56*, 476-496.